Available online at www.sciencedirect.com

ScienceDirect

Geochimica et Cosmochimica Acta 195 (2016) 244–258

Geochimica et Cosmochimica Acta

www.elsevier.com/locate/gca

In situ thermal characterization of cooling/crystallizing lavas during rheology measurements and implications for lava flow emplacement

S. Kolzenburg [a,*], D. Giordano [a], C. Cimarelli [b], D.B. Dingwell [b]

[a] *Dipartimento di Scienze della Terra, Universita degli Studi di Torino, 10125 Torino, Italy*
[b] *Department für Geo-und Umweltwissenschaften, Ludwig-Maximilians-Universität, 80333 München, Germany*

Received 27 January 2016; accepted in revised form 18 September 2016; available online 23 September 2016

Abstract

Transport properties of natural silicate melts at super-liquidus temperatures are reasonably well understood. However, migration and transport of silicate melts in the Earth's crust and at its surface generally occur at sub-liquidus temperatures and in settings where the melts undergo crystallization under various cooling and/or decompression conditions. In such dynamic situations the occurrence of processes such as the release of latent heat during phase changes, viscous heating, thermal advection and -inertia, and changing heat capacity, all represent potential influences on the state, and thereby on the physico-chemical behavior of the system. To date, rheological data at sub-liquidus temperatures are scarce and cooling-rate dependent, disequilibrium rheological data are virtually absent. In fact, no *in situ* thermal characterization of liquid or multiphase mixtures during rheological experiments, under either static or dynamic thermal conditions has been presented to date.

Here we describe a new experimental setup for *in situ* thermal characterization of cooling/crystallizing lavas *during* viscosity measurement at temperatures up to 1600 °C. We use this device to recover *in situ*, real-time, observations of the combined rheological and thermal evolution of natural, re-melted lava samples during the transient disequilibrium conditions characteristic of lava flows and shallow crustal magma migration and storage systems in nature.

We present the calibration procedure and the method employed to recover the thermal evolution of an experimental sample during flow in varying shear regimes, assess the experimental uncertainty and show the ability of the apparatus to measure the release of latent heat of crystallization during transient rheological experiments. We further report the results from a first experimental study on the rheological and thermal evolution of a basaltic lava undergoing continuous cooling at a series of different cooling rates and discuss the implications of the results for magma migration and lava flow emplacement.

Keywords: Rheology of Magmatic Suspensions; Concentric Cylinder; Viscometry; Temperature; Latent Heat; Crystallization; Spindle; Disequilibrium Processes

* Corresponding author.
E-mail address: skolzenburg@gmail.com (S. Kolzenburg).

http://dx.doi.org/10.1016/j.gca.2016.09.022
0016-7037/

1. INTRODUCTION

1.1. Disequilibrium transport conditions in natural environments

The rheology of lava and magma is one of the key parameters governing the emplacement of lava flows and the migration of melts in the Earth's crust. Both pāhoehoe and 'A'ā flows are spatially restricted in their flow paths by the increasing strength of a growing crust, and/or high viscosity zone (Calvari and Pinkerton, 1998; Kauahikaua et al., 1998; Hon et al., 2003; Cashman et al., 2013; Castruccio and Contreras, 2016). The influence of the dynamic rheology of lava on its style of emplacement becomes especially evident in the late stages of the flow, where its resistance to flow becomes stronger and its exterior is subjected to folding and fracturing. Viscosity gradients resulting from the differential cooling of the lava surface and its interior play a significant role in the generation of flow-directing features like levees and lava tubes (Sparks et al., 1976; Lipman and Banks, 1987) as well as the sealing of dikes through heat loss at the contact with the country rock (Giordano et al., 2007).

Measurements of the flow properties of natural lavas in the field have been previously reported in the literature (Shaw et al., 1968; Pinkerton and Sparks, 1978; Pinkerton and Norton, 1995). Albeit being crucial measurements for benchmarking of experimental data, these do not allow for a systematic study on the evolution of flow properties in temperature or shear rate space.

Maximum temperatures in lava flows and active lava tubes may reach beyond 1280 °C (Flynn and Mouginis-Mark, 1994; Kauahikaua et al., 1998). Such extreme temperatures, seemingly unexpected for lavas commonly erupting at lower temperatures (generally between 1100 and 1200 °C and below), may be reached through combustion of gases released by the magma (Peterson and Swanson, 1974; Kauahikaua et al., 1998) or by viscous heating (Costa and Macedonio, 2005b).

Cooling rates of basaltic lavas, measured at the surface and within active lava channels during emplacement at a variety of locations (dominantly Hawaii, due to the relatively easy access and availability of supporting infrastructure), range from 0.01 to 15 °C/min (Flynn and Mouginis-Mark, 1992; Hon et al., 1994; Cashman et al., 1999; Witter and Harris, 2007). Cooling rates have also been evaluated through theoretical studies based on the flow geometry and crystal structures of komatiites lavas at 1–21 °C/min (Huppert et al., 1984). These values, most of which are representative for the exterior part of lava flows, can be taken as maximum cooling rates and are lower in the interior of the lava flow.

Narrow and shallow dikes may undergo cooling rates from few degrees per hour to more than 50 K/min, as the magma is introduced into a fracture; see Giordano et al. (2007) for the case of the Nyiragongo 2002 eruption. Cooling rates then decrease as a function of the size of the dike and time. After the transient stages (a few hours) magma in narrow dikes undergo cooling rates of the order of ca. 5 K/min or less.

The importance of *disequilibrium* effects on the crystallization kinetics and textural development of silicate melts has been recognized for decades (Walker et al., 1976; Pinkerton and Sparks, 1978; Coish and Taylor, 1979; Gamble and Taylor, 1980; Lofgren, 1980; Long and Wood, 1986; Hammer, 2006; Giordano et al., 2007; Arzilli and Carroll, 2013; Vetere et al., 2013). Yet, only a few experimental studies investigating the cooling- or shear-rate dependence of the transport properties of crystallizing silicate melts have been presented to date (Shaw et al., 1968; Kouchi et al., 1986; Ryerson et al., 1988a; Giordano et al., 2007).

In this manuscript we present viscosity measurements and differential thermal analysis data from experiments carried out under disequilibrium, mimicking natural conditions. The goal is to more accurately describe the flow properties of lavas and magmas under dynamic thermal conditions, pertinent to nature.

1.2. Experimental measurements of subliquidus rheology in magmatic systems

Concentric cylinder viscometry represents a widely-applied technique for measuring the viscosity of silicate melts at super-liquidus temperatures (Dingwell and Virgo, 1988; Dingwell, 1989; Webb and Dingwell, 1990; Mauro et al., 2009). In combination with either low temperature measurements, e.g. via micro-penetration viscometry (Hess et al., 1995; Hess and Dingwell, 1996) or estimation of the melt viscosity by application of a shift factor to scanning calorimetry data (Stevenson et al., 1995; Gottsmann et al., 2002; Giordano et al., 2008a), these data can be used to interpolate the temperature-dependent viscosity of a pure liquid at sub-liquidus temperatures (Hess et al., 1995; Hess and Dingwell, 1996; Gottsmann et al., 2002; Russell et al., 2002, 2003; Hui and Zhang, 2007; Giordano et al., 2008a). Recent studies have applied these experimental methods to measure the rheological evolution of silicate melts subjected to isothermal sub-liquidus conditions, where crystallization takes place (Ryerson et al., 1988a; Stein and Spera, 1992; Hoover et al., 2001; Sato, 2005; Ishibashi and Sato, 2007; Ishibashi, 2009; Vona et al., 2011, 2013; Robert et al., 2014; Sehlke et al., 2014; Chevrel et al., 2015; Sehlke and Whittington, 2015; Campagnola et al., 2016; Soldati et al., 2016). However, non-isothermal rheological data on natural melts are virtually absent in the literature.

Concentric cylinder viscometry uses the torque exerted by the liquid on a spindle inserted into a melt while rotated at a constant rate to determine the viscosity of the sample. Accurate calibration of temperature measurements at these experimental conditions ($P = 1$ atm; $T = \sim 900$–1600 °C) requires the insertion of a thermocouple (commonly PtRh Type S or B) into the sample. To date, this has been hindered in rotational viscometry, as data transmission relied on wired connections, compromising the highly sensitive torque measurement needed for accurate viscosity determination.

In temperature-stepping experiments (i.e. stepping between isothermal conditions) this issue can be overcome by calibrating the sample temperature against the furnace

temperature; e.g. (Dingwell, 1986). This becomes increasingly difficult during constant cooling rate experiments as thermal inertia can affect the measurement system. Crystallization, viscous heating, redox foaming, heat advection and changing heat capacity may also influence heat loss from the sample and therefore its thermal state. Further, static temperature calibration (without stirring) cannot assess the presence and magnitude of viscous-heating effects potentially acting at high viscosities or high shear rates (Hess et al., 2008; Cordonnier et al., 2012) or the release of latent heat of crystallization, e.g. (Settle, 1979; Lange et al., 1994; Blundy et al., 2006) at sub-liquidus conditions and varying shear rates.

In this manuscript we introduce a newly designed spindle that enables direct measurement of the temperature and its vertical gradient within an experimental sample *during* concentric–cylinder viscometry through the use of wireless data transmitters. This represents a significant expansion of experimental capabilities for the accurate description of high temperature rheology, enabling accurate measurements under transient disequilibrium conditions. We present experimental data from viscosity and temperature calibrations of the setup as well as data from experiments on natural samples that assess the release of latent heat during crystallization of a sample under constant cooling conditions.

The conditions imposed in the presented experiments, starting at super-liquidus temperatures and imposing cooling rates between 0.5 and 5 °C/min cooling, represent the rapid to intermediate cooling rates which are present in the interior of high aspect ratio (i.e. sheet-like) lava flows and the lava carapace as well as the conditions of migrating magmas at shallow depths.

2. EXPERIMENTAL APPARATUS

2.1. Spindle design and setup

The new spindle is used in combination with the experimental setup described in Dingwell (1986) and Dingwell and Virgo (1987) which consists of a Deltech®, bottom-loading, box furnace with an upper temperature limit of 1700 °C (Fig. 1). The furnace has a hole in the top

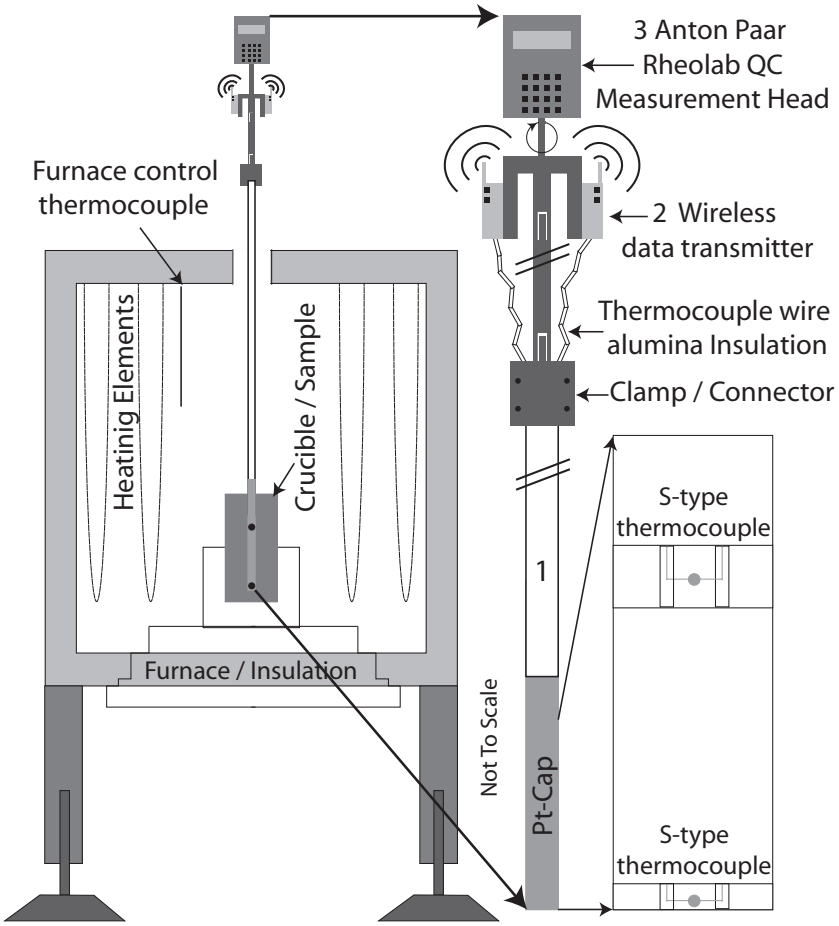

Fig. 1. Sketch of the new spindle and supporting hardware. (Not to scale) Left: A cross section through the experimental setup. The sample is loaded from the bottom of the furnace and is contained in a $Pt_{80}Rh_{20}$ crucible housed in an insulating brick in the hot zone of the furnace. The spindle is introduced into the sample through a hole in the top of the furnace. The furnace temperature is controlled via an independent thermocouple suspended in the hot zone. Right: The alumina spindle (1) is connected to the Rheometer head using jointed rods. The final jointed rod (2) is connected to the two UWTC1 wireless data transmitters (3). The entire spindle setup rotates during measurement and, therefore, data transmission does not compromise the torque measurements. The enlargement shows a sketch of the tip of the alumina rod that is cut open at its end and at 30 mm height in order to house the thermocouple welding beads.

insulation plate that allows introduction of the spindle used for viscosity measurements into the sample. This setup is located at both the Earth and Environmental Sciences department of the University of Munich and, similarly, at the *Geomatlab* of the Earth Sciences department of the University of Turin.

The spindle is attached to an Anton Paar Rheolab QC® rheometer head with a torque range of 0.25–75 mN·m and a rotational velocity range of 0.01–1200 rpm. It is composed of an 8 mm diameter alumina ceramic rod with four 1.5 mm diameter holes along its long axis. These holes house the S-type thermocouple wire. Given the crucible diameter of 26.6 mm this geometry results in a gap width of 9.3 mm. The ceramic rod was cut open at 30 mm from its lower end in order to host one of the two S-type thermocouples. The second S-type thermocouple weld is located at the lower tip of the spindle, where the separating wall between two channels was ground back slightly (Fig. 1). After installation of the thermocouples, the measuring end of the spindle, that is to be inserted in the sample melt, is sheathed with Pt tubing and welded shut. This avoids contamination of the sample or the thermocouple during the measurement. A 0.2 mm alumina ceramic plate is installed on the inside of the base of the end cap as well as the side wall near the second thermocouple. This ensures electrical and mechanical insulation of the thermocouple weld from the Pt-cover. This Pt-cover is secured to the alumina rod with 0.5 mm Pt wire, using a thin bore through the spindle center. The thermocouple wires, electrically insulated by thin (1.5 mm diameter; 0.1 mm wall thickness) ceramic tubes, are led out of the top of the spindle and connected to an OMEGA® UWTC1 wireless data transmitter. These data transmitters are attached to a light weight bar that is rotating on the spindle axis (Fig. 1). This setup has no influence on the torque measured by the rheometer head.

2.2. Calibration procedure

The temperature readings of both thermocouples within the spindle were calibrated against an external, Pt-sheathed, type-S thermocouple inserted directly into the melt for temperatures between 950 and 1450 °C. Calibration was performed by dropping the furnace temperature in steps of 50 °C and equilibrating the sample for a minimum of two hours. The accuracy of the temperature reading was within the measurement uncertainty of a type-S thermocouple of ±1 °C. We do, however, find that there is a stable thermal gradient within the sample of <4 °C, where the top of the sample is slightly hotter than its bottom. This thermal gradient is largest at low temperatures (below ~1100 °C) and decreases to <2.5 °C at higher temperatures. The gradient is stable on the timescale of hours to days and is a result of the setup geometry (with the top of the crucible being more directly exposed to the thermal radiation of the heating elements of the furnace, see Fig. 1). This geometry is optimized to achieve a minimal thermal gradient, while maintaining mechanical integrity (i.e. a stable and secure crucible fit in the ceramic-brick). The temperature calibration results are summarized in Fig. 2A. The temperatures of both top and bottom thermocouple are plotted together with the set point of the furnace controller (controlled by a type B thermocouple located within the furnace; see Fig. 1).

The spindle head used in these experiments is cylindrical (60 mm long; 8 mm diameter). Experiments are conducted by immersing the spindle into the melt over a length of

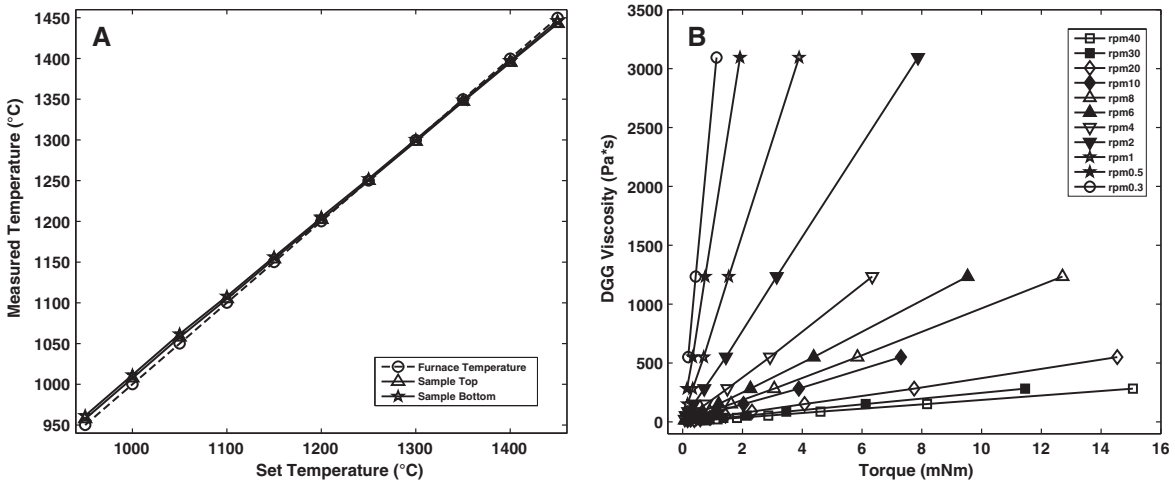

Fig. 2. Summary of the calibration data. (A) Temperature calibration. The dashed line shows the furnace set temperature (controlled by a type-B thermocouple located in the hot zone of the furnace). Solid lines show the measured sample temperature at the top and bottom (triangles and stars, respectively) of the sample. Note, that there is a small (<4 °C) thermal gradient within the sample that decreases with increasing temperature. Also, note that the average sample temperature is higher than the furnace set temperature for values below 1200 °C, whereas above 1200 °C the sample is slightly cooler than the set temperature. (B) Raw data from the torque-viscosity calibration. Each symbol represents a steady torque value measured at the respective constant rotation-rate and a constant melt viscosity of the calibration standard. Increasing shear rate results in constantly decreasing slope of the torque-viscosity relationship. Linear fits to this data, forced through the origin, are used to convert the measured torques to sample viscosity (or apparent viscosity for suspensions). R^2 values for these fits are higher than 0.9988.

45 mm. The torque-viscosity-calibration was performed over a temperature range from 970 to 1450 °C at rotation rates from 0.3 to 40 rpm (Fig. 2B), corresponding to strain-rates of ca. 0.07–9.3 s^{-1}. The torque reading of the device is calibrated (at a range of rotation rates) to the viscosity of the DGG-1 standard melt (Fig. 2B) for which the viscosity-temperature relationship is accurately known (Meerlender, 1975). Consequently, using linear fits to the calibration data, a torque measurement at a certain rotation rate corresponds to the viscosity of an unknown melt. The R^2 values of these linear fits (while forcing the fit through the origin to capture the largest possible error) are larger than 0.9988.

The maximum influence of the temperature gradient of <4 °C within the sample (described above) on the viscosity calibration is assessed by determining its effect on the viscosity of DGG-1 at various temperatures. We use an average temperature reading of the two thermocouples to calculate the melt viscosity of DGG-1 and based on these calculations we can ascribe an accuracy of the viscosity measurement of better than ±0.04 log units.

2.3. Differential thermal analysis during concentric cylinder rheometry

Our newly built setup allows *in situ* measurements of the sample temperature over the entire course of the experiment. Temperature sampling rate is set at 5 Hz during all experiments. Type-S thermocouples have an inherent measurement uncertainty of ±1 °C and the noise in the recorded data has, therefore, been smoothed by calculating the moving average over 60 data points. A sample experiment on a basaltic melt undergoing crystallization is shown in Fig. 3A. The data show that when imposing a constant cooling rate to the box furnace controller, the sample shows an initial thermal lag (highlighted with a gray circle in Fig. 3A). This delay is the result of the thermal inertia of the melt within the experimental crucible and the ceramic brick housing the crucible. After passing through the thermal lag, the sample enters a phase of constant cooling at the same rate as set for the furnace but at slightly elevated absolute temperature. Crystallization of the basaltic sample occurs at temperatures below 1200 °C and the measured temperature departs to higher values than expected for a linear cooling path (see insert in Fig. 3A).

In order to estimate the intensity and nature of this departure, we extrapolate the linear cooling path of the melt (at super-liquidus temperatures discarding those data points affected by the initial thermal lag) using a linear model and then normalize the recorded sample temperatures to this model (Fig. 3A). Data for both the basalt and DGG-1 are reported in Fig. 3B. The DGG-1 sample, which does not crystallize under the imposed conditions, follows the extrapolated model within the measurement uncertainty of the thermocouple, whereas the crystallizing basaltic sample departs significantly from the linear model. The data in Fig. 3B validate our extrapolation technique and all results will be reported as a ΔT between the crystallizing melt and the extrapolated cooling model from here on.

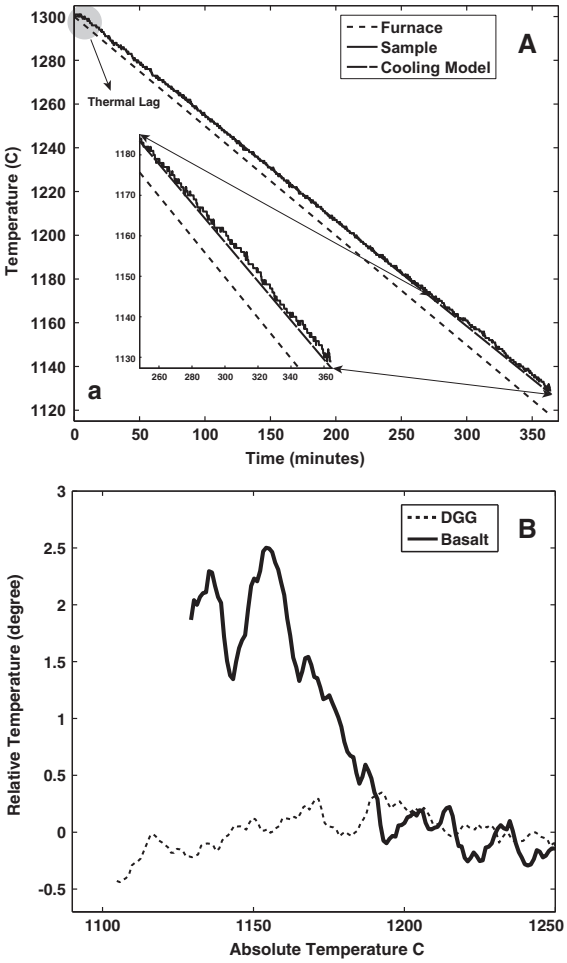

Fig. 3. Thermal characterization of the sample. (A) Example of a thermal path for a constant cooling rate experiment where the sample undergoes crystallization. The initial thermal lag between furnace and sample is highlighted in the top left. Inset in panel A shows a zoom on the release of thermal energy with respect to the linear extrapolation of the super-liquidus cooling path. Note the deviation from linear cooling towards the end of the experiment, representing the relative heating of the sample with respect to its imposed cooling conditions. Albeit small, the deviation is significant. This becomes more apparent when normalized to the cooling model of the liquid. (B) Results from the differential thermal analysis. A comparison between tests performed on a non-crystallizing DGG-1 standard sample (dashed line) and a crystallizing basaltic sample (solid line) show how accurately the differential thermal analysis approach resolves the release of latent heat of crystallization.

3. SAMPLE PREPARATION AND EXPERIMENTAL METHOD

3.1. Sample composition and geologic relevance

We chose a primitive basaltic melt for these experiments (see Table 1 for the chemical composition). This composition is representative of a large fraction of melts erupted at divergent continental margins, representing ~80% of all volcanism on Earth. Fig. 4 shows a TAS diagram, where

Table 1
Chemical analysis: Weight% oxides for the experimental sample before and after the crystallization experiments, normalized to 100%.

Oxide	*Pre*	*Post*
SiO_2	48.86	48.92
TiO_2	1.86	1.88
Al_2O_3	13.29	13.19
Fe_2O_3	15.01	14.94
MnO	0.00	0.00
MgO	6.81	6.85
CaO	11.87	11.85
Na_2O	2.26	2.29
K_2O	0.04	0.08
P_2O_5	0.00	0.00

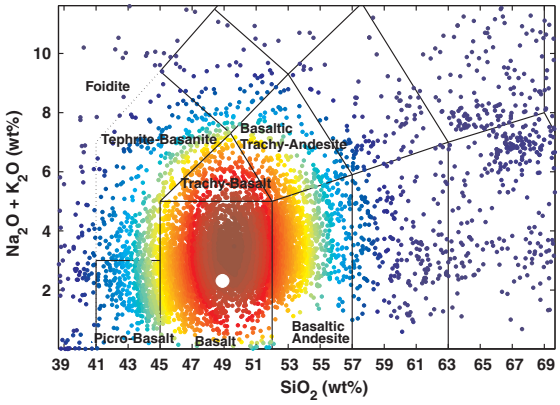

Fig. 4. TAS diagram. TAS diagram of the sample composition (white dot) and ~9500 geochemical analyses of samples from divergent margins and Large Igneous Provinces. The example data stem from the north- and central-Atlantic Igneous-provinces, the Deccan traps, the east African rift and the Parana-Etendeka flood basalts. Geochemical data was taken from the GEOEC database (Sarbas and Nohl, 2008) of the University of Mainz and color coded for data density. Note, that the sample chosen for these experiments plots near the center of the highest data density for these geologic settings.

the experimental melt composition is plotted in reference to ~9.500 geochemical analyses of rocks from the north- and central-Atlantic-igneous-provinces, the east African rift, the Deccan traps and the Parana-Etendeka flood basalts. The data are taken from the GEOROC database of the University of Mainz (Sarbas and Nohl, 2008) and are color coded for data density. The dominant fraction of the geochemical analyses from these examples of divergent margin settings and flood basalt provinces plot around the composition of the experimental sample. Further, both the cooling- and shear-rates imposed during the experiments are common to lava and magma emplacement in these geologic settings. The presented data can, therefore, be used in the interpretation of globally relevant magmatic and volcanic processes in these settings. We do acknowledge however, that the range of cooling- and shear-rates present in nature, e.g. during lava flow emplacement (Wright and Okamura, 1977; Harris et al., 2005, 2007; Witter and Harris, 2007), spans a wider range than what is technically possible to reproduce in the laboratory.

3.2. Sample preparation

The rock samples are crushed and powdered using a jaw crusher and carbide ring-mill to create rock powders suitable for melting. The powders are then melted in large (100 ml), thin-walled, Pt crucibles. Melting is performed in a Nabertherm® $MoSi_2$ box furnace at 1250 °C in batches of ~10 g, added to the crucible every 5 min. This avoids overflow of the melt due to foaming. Rock powders vesiculate during synthesis and produce a bubbly melt that loses most of its vesicles after 20 min at 1250 °C. Vesiculation is likely due to a combination of the presence of moisture in the rock powder, the exsolution of volatiles from the partially glassy rock and the liberation of oxygen bubbles as the melt undergoes a change in redox state at high temperature (Kress and Carmichael, 1991). Once completely filled, the crucible is left in the furnace for about an hour in order to allow for the melt to degas. Degassing is completed after this time and no visible bubbles remained in the melt or on its surface. The samples are quenched to glasses by pouring them onto a steel plate. The glasses are then crushed and remelted into $Pt_{80}Rh_{20}$ cylindrical crucibles of 51 mm height and 26.6 mm diameter for rheological investigations.

3.3. Concentric cylinder experiments

The samples are stirred at a constant temperature of 1294 °C (corresponding to a furnace set point of 1300 °C) for several hours to ensure chemical and thermal homogeneity, which is confirmed by a steady torque and constant temperature reading. The furnace temperature is then decreased in steps of 20 °C and held until a steady temperature and torque reading is achieved for each step (typically 45 min). These data are used to recover the samples' superliquidus viscosity at each temperature step.

The same basaltic sample used to measure pure liquid viscosity at isothermal conditions is also used for subliquidus experiments. Measurements are performed by imposing a constant cooling rate of 0.5, 1, 3 and 5 °C/min and a mean initial shear rate of 4.642 s^{-1} (corresponding to 20 rpm). During the cooling experiments the measured torque constantly increases as a function of the apparent viscosity of the suspension. In order to ensure mechanical stability of the crucible in its ceramic holder, a torque limit of 5 mN·m is set and the shear rate is automatically dropped to 2.321, 1.857, 1.393, 0.928, 0.464, 0.232, 0.116 s^{-1} (10, 8, 6, 4, 2, 1, 0.5 rpm, respectively), every time this limit is reached.

After each constant cooling rate experiment, and before running the next one, the sample is re-heated to 1294 °C for a minimum of two hours and homogenized by stirring at the initial shear rate (4.642 s^{-1}) in order to ensure melting of the crystalline phases formed during previous experimentation. Thermal equilibration is reached after ~1 h and remelting of previous crystalline phases is confirmed by the recovery of a steady torque measurement equivalent to the value of the pure melt over more than an hour. Mysen and Virgo (1978) report complete redox equilibration in droplet-sized samples of iron rich silicate melts to occur within less than 30 min, whereas Dingwell and

Virgo (1987) and Dingwell (1991) find that for sample of the same volume as used in this study, complete equilibration may take up to 24 h for samples with slightly higher iron contents than the ones used here. Chevrel et al. (2013) measured iron-rich basaltic analogs for Martian melts and report equilibration after 24 h. We therefore assume that, initially, redox equilibrium is achieved during the super-liquidus melt viscosity determination, which lasted more than 24 h at atmospheric conditions. Subsequent crystallization experiments last between 0.5 and less than 6.5 h (at lower temperatures, i.e. higher viscosities and slower redox equilibration) and we therefore assume that the melt's redox state re-equilibrated to the initial, pre-experimental state within the two hours spent at high temperature under constant stirring. This assumption is supported by the observation that torque values measured after rehomogenization between and after all experimental runs stabilize with a reproducibility of 0.005 mN·m (~1.5% of the measured value). The sample used for all the constant cooling rate experiments is re-melted and quenched to a glass after the end of the last cycle.

The composition of the samples before and after viscosity measurements is determined by Electron Microprobe Analysis (EMPA) at the University of Torino, Department of Earth Sciences using a Cambridge S-360 equipped with Oxford INCA Energy 200 and X-act SDD Detectors. Energy dispersive spectra are recorded and processed using Oxford Instruments INCA® analyzer software. The probe is operated at 1.22 nA with a 15 keV acceleration voltage using a defocussed 10 μm diameter spot to avoid loss of volatile elements (such as K, Na and Cl). Normalized analysis results are presented in Table 1; analytical totals are 99.24% and 98.54% for the pre and post experimental glass, respectively. Data presented here have standard deviations for all elements less than ±2.5%.

3.4. Estimation of low temperature viscosity

In order to reconstruct the full range of temperature-dependent viscosity of the melt, we use the model of Giordano et al. (2008b) to estimate the melt viscosity at lower temperatures. This model has been shown to work well for estimating the viscosity of basaltic compositions (Ishibashi, 2009; Giordano et al., 2010; Vona et al., 2011; Chevrel et al., 2013).

The effect of the changing residual melt composition on the viscosity is estimated to be within 0.01–0.03 log units at 900 °C and less at higher temperatures (0.2 log units at the rheological cut-off). These results are based on calculations of the residual melt composition, starting from the composition of the original sample. We used MELTS software for estimations of the composition of a dry melt at 1130 °C and a crystal fraction of 53.5 vol.% as well as for a dry melt at 1150 °C and a crystal fraction of 37.5 vol.%. These temperatures correspond to the interval where we observe the largest deviation in viscosity (i.e. most intense crystallization) in our experiments. We then model the residual melts viscosity-temperature relationship using Giordano et al. (2008b). The difference in viscosity between the original and residual melt increases with decreasing temperature. These model results are in good agreement with values measured by Vona et al. (2011) and Giordano et al. (2010) who estimated values of 0.06–0.18 log units difference between original and residual melt viscosities for experiments on basaltic melts from Stromboli and Etna.

Measured and modeled values for the high temperature viscosity are accurate to less than 0.2 log units. We therefore use 0.2 log units as the uncertainty on the low temperature viscosity estimates recovered from the GRD model for interpolation of the viscosity data over the entire experimental temperature interval.

4. RESULTS

4.1. Liquid viscosity

The results of the pure liquid viscosity measurements for high temperature viscometry and low temperature model estimates are summarized in Table 2 and plotted in Fig. 5A together with the fit parameters for a Vogel–Fulcher–Tammann (VFT) equation (Tammann and Hesse, 1926) fitted to these data. This VFT fit describes the theoretical behavior of the melt in viscosity-temperature space if no crystallization were to occur. No constant torque reading was achieved for temperatures below 1214 °C, suggesting slow crystallization of the sample. Since these data would no longer be a measure of pure melt viscosity but of a melt plus crystal suspension, data for temperatures below 1214 °C were discarded. This observation is in reasonable agreement with equilibrium liquidus temperature of ~1196 °C estimated for this composition using the MELTS software (Gualda and Ghiorso, 2015).

4.2. Dynamic crystallization experiments

Fig. 5B shows a summary of the apparent viscosity measurements at different cooling rates and the VFT-fit curve to the pure liquid data (dotted line). Above the liquidus

Table 2
Summary of liquid viscosity measurements (high temperatures) and model estimates of the low temperature viscosity of the melt (stars) as well as VFT-fit parameters.

Temperature (K)	log10 viscosity (Pa s)	Associated uncertainty in log units
1567	0.96	0.02
1547	1.06	0.02
1528	1.16	0.02
1507	1.29	0.02
1488	1.40	0.02
938*	12.26	0.20
944*	11.95	0.20
946*	11.84	0.20
966*	10.89	0.20
975*	10.49	0.20
978*	10.37	0.20
A	−3.80	
B	4226.45	
C	676.75	

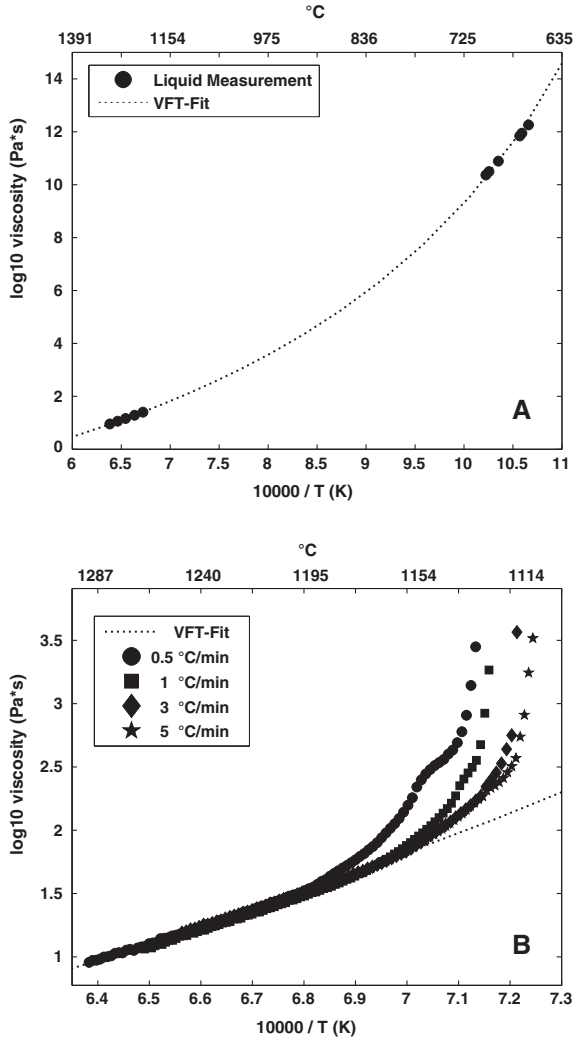

Fig. 5. Absolute viscosity data. (A) High temperature melt viscosity measurements, low temperature viscosity estimates and VFT-Model of the theoretical viscosity-temperature relationship of the sample. (B) Summary of the absolute viscosity measurements from dynamic crystallization experiments at varying cooling rates. Note that all samples follow the VFT model up until the point where the presence of crystals becomes significant enough to influence the flow behavior of the sample. The temperatures of this initial departure, as well as the "cut-off" temperature where the system's apparent viscosity exponentially increases towards infinity, are decreasing with increasing cooling rate.

temperature, all data follow the pure liquid viscosity trend. At temperatures below the liquidus, the experimental data deviate from this trend at different degrees of undercooling, depending on the applied cooling rate. This departure from the VFT-fit (representing the theoretical viscosity-temperature evolution of the crystal free liquid) shifts to higher temperatures with decreasing cooling rate. Data for cooling rates of 3 and 5 °C/min follow the liquid trend to the lowest cut-off temperatures among those recorded during our experiments. These data initially deviate along the same path. At lower temperatures the experiment cooled at 5 °C/min remains at lower apparent viscosities than the one cooled at 3 °C/min. When the cooling rate decreases further, the deviations become more pronounced and the data diverge more drastically. All datasets show a stage of decreasing acceleration of this departure that is discussed in detail in (§ 4.3). Using the VFT-model (§ 4.1) for the temperature dependent viscosity of the theoretical pure liquid we calculate the suspensions' relative viscosity. This is done by normalizing the data of the crystallization experiments to the VFT-fit using the following equation to recover the system's relative viscosity:

$$\eta_r = \frac{\eta_s}{\eta_l} \tag{1}$$

where η_r, η_s and η_l are the relative viscosity, the viscosity of the suspension (i.e. liquid plus crystals in the crystallizing sample) and the liquid viscosity, respectively. This enabled us to resolve the crystallization-induced departure from the original pure liquid properties in greater detail than by just considering the variations in absolute viscosity. The results of the rheological and thermal measurements during all constant-cooling experiments are summarized in Fig. 6A–D. The experimental data of the crystallizing system as it changes from a pure liquid to a liquid–solid suspension are reported both in terms of absolute and log relative viscosity in Table 3.

The temperature-dependent viscosity of the melt, when subjected to varying cooling rates, initially follows the trend of the pure liquid data (and extrapolated VFT fit for the supercooled liquid), resulting in a zero (0) log (relative viscosity). Once the crystallinity (via nucleation and growth of crystals) becomes high enough to measurably influence the viscosity the data deviate from zero. At this point the apparent viscosity of the suspension increases with respect to the theoretical liquid as a result of increasing crystal content and changing composition of the residual melt. The latter has been estimated to be below 0.03 log units, as discussed above (§ 3.4). The relative viscosity initially increases slowly with decreasing temperature for all experiments (Fig. 6A–D). This increase steepens rapidly as temperature decreases further. However, this steepening is retarded for thermal intervals of varying widths (plateau width increases with decreasing cooling rate). This effect is most prominent for cooling rates of 5, 1 and 0.5 °C/min (Fig 6A, B and D). Decreasing temperature further, the relative viscosity increases again strongly until the measurement limit of the experiment is reached. These changes in relative viscosity are directly linked to the intensity of crystallization, as increases in relative viscosity result from a larger fraction of crystals impeding flow. These changes in crystallization intensity recorded in the viscosity data become even more evident when plotting the derivatives of the relative viscosity as a function of temperature (Fig. 7). The onset (local minimum) and center (local maximum) of the plateaus in the relative viscosity are resulting from a decrease in crystallization intensity (e.g. lowering crystal growth rates over the respective temperature intervals). They occur at decreasing absolute temperatures with increasing cooling-rate. These discontinuous variations in the crystallization-driven increase of the apparent viscosity of the suspension can, with the new experimental device, be

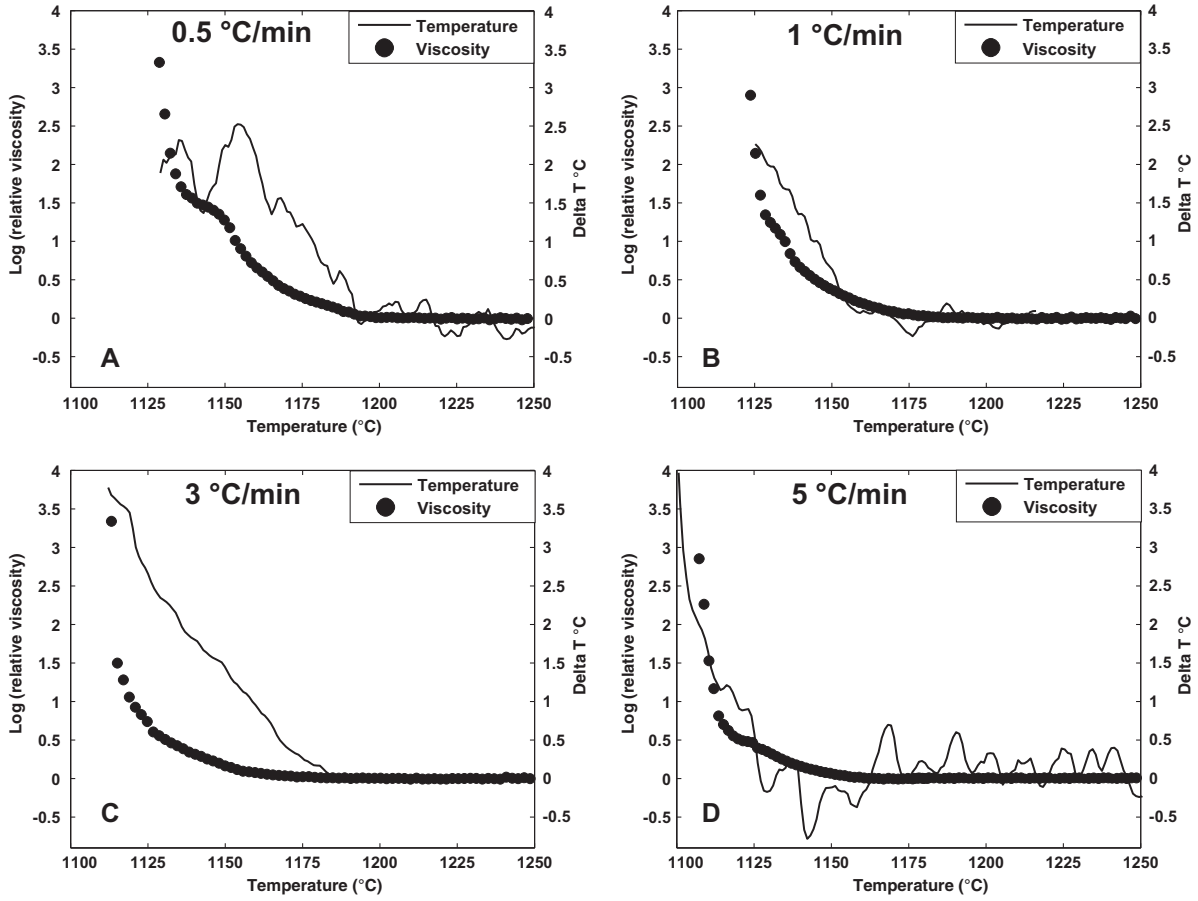

Fig. 6. Evolution of relative viscosity and temperature of crystallizing samples. Summary of rheological (black dots) and thermal (black line) evolution of the sample plotted as relative viscosity and -temperature for each imposed cooling rate. Note that the initial rheological and thermal departure and the "cut-off" temperature are directly coupled and are decreasing with increasing cooling rate. Note also, that decreases in the release of thermal energy are linked to a plateau in relative viscosity. In these sections, the relative viscosity of the suspension is no longer increasing (although the absolute apparent viscosity is, as a result of the temperature dependence of the viscosity of the interstitial melt) since crystal growth has slowed down or halted. This is especially prominent for the slowest (0.5 °C/min) cooling rate (panel A).

directly related to the thermal response resulting from changes in the crystallization intensity. The data show a cooling-rate dependence of this departure, whereby slower cooling results in a departure from the theoretical liquid at higher temperature. This is in good agreement with earlier experiments by Giordano et al. (2007) who performed constant cooling rate experiments on natural, foiditic melts from Nyiragongo, DRC.

4.3. Thermal evolution of the samples during crystallization

Figs. 6A–D illustrate the evolution of the relative sample temperature and the logarithm of the relative viscosity for each individual constant cooling rate experiment. For all experiments, the intensity of heat release during crystallization is directly correlated to an increasing relative viscosity. For any given cooling rate, increases in the relative viscosity and in relative sample temperature (with respect to the imposed cooling path) occur simultaneously. This verifies that both the viscosity measurement and the differential thermal analysis detect the onset of crystallization of the melt well. The onsets of the release of thermal energy as well as the onset of the rheological departure from the pure melt, however, shift to lower temperatures with increasing cooling rate (Figs. 5 and 6). The intensity of the heat release increases with increasing cooling rate, since it is directly coupled to increasing nucleation- and growth-rates of crystals with increased undercooling of the sample (Mollo et al., 2011; Arzilli and Carroll, 2013). As demonstrated most clearly by the dataset at the slowest cooling rate (Fig. 5A), the release of thermal energy during crystallization is not constant with decreasing temperature. Instead, it undergoes an initial strong increase and then decreases over a short temperature interval to finally accelerate once again at lower temperatures (i.e. higher undercooling). These changes in the crystallization intensity are directly related to the rheological response of the suspension; i.e., all changes in the viscosity data can directly be linked to the crystallization kinetics of the system. During crystallization the suspension viscosity increases due to the increasing crystal content. However, the release of latent heat of crystallization increases the temperature of the interstitial melt,

Table 3
Summary of absolute and relative viscosity measurements for all experiments. For simplicity, interpolated values of the experimental data at equal temperature steps are reported with exception of the final datapoint for each experiment. Temperatures related to those points are reported in the last two rows in Kelvin and Celsius, respectively.

	Cooling rate	0.5 K/min		1 K/min		3 K/min		5 K/min	
Temperature (K)	Temperature (C)	Absolute Viscosity (log10 Pa s)	Relative Viscosity (log10 Pa s)	Absolute Viscosity (log10 Pa s)	Relative Viscosity (log10 Pa s)	Absolute Viscosity (log10 Pa s)	Relative Viscosity (log10 Pa s)	Absolute Viscosity (log10 Pa s)	Relative Viscosity (log10 Pa s)
1523	1250	1.19	0.00	1.17	0.01	1.19	−0.01	1.18	0.00
1518	1245	1.22	0.00	1.19	−0.01	1.22	0.00	1.20	0.00
1513	1240	1.25	0.01	1.21	−0.01	1.25	0.01	1.23	0.00
1508	1235	1.27	−0.01	1.25	0.00	1.28	0.00	1.26	0.00
1503	1230	1.30	−0.01	1.27	−0.01	1.31	0.00	1.29	0.00
1498	1225	1.34	−0.01	1.30	−0.02	1.34	0.00	1.32	−0.01
1493	1220	1.36	−0.01	1.34	−0.01	1.37	−0.01	1.35	−0.01
1488	1215	1.40	0.00	1.37	−0.01	1.40	−0.01	1.38	−0.01
1483	1210	1.44	0.01	1.40	−0.01	1.43	−0.01	1.41	−0.01
1478	1205	1.47	0.01	1.43	0.00	1.46	0.00	1.45	0.00
1473	1200	1.50	0.01	1.46	0.00	1.50	0.01	1.48	0.00
1468	1195	1.54	0.03	1.50	0.01	1.53	0.01	1.51	0.01
1463	1190	1.60	0.08	1.53	0.01	1.56	0.00	1.55	0.01
1458	1185	1.66	0.15	1.57	0.01	1.60	0.01	1.58	0.01
1453	1180	1.72	0.21	1.61	0.03	1.63	0.01	1.62	0.00
1448	1175	1.79	0.28	1.66	0.06	1.67	0.02	1.66	0.00
1443	1170	1.86	0.37	1.70	0.09	1.71	0.04	1.70	0.00
1438	1165	1.96	0.51	1.76	0.14	1.75	0.05	1.75	0.00
1433	1160	2.06	0.67	1.82	0.19	1.80	0.08	1.80	0.01
1428	1155	2.20	0.91	1.89	0.28	1.84	0.10	1.85	0.03
1423	1150	2.40	1.27	1.97	0.38	1.91	0.17	1.91	0.07
1418	1145	2.51	1.44	2.06	0.50	1.98	0.24	1.97	0.11
1413	1140	2.59	1.54	2.17	0.66	2.05	0.32	2.04	0.16
1408	1135	2.73	1.79	2.35	1.00	2.13	0.42	2.12	0.24
1403	1130	3.25	2.90	2.50	1.26	2.21	0.53	2.21	0.34
1398	1125	3.45	3.33	3.01	2.33	2.34	0.74	2.30	0.45
1393	1120			3.27	2.90	2.49	0.98	2.38	0.51
1388	1115					2.80	1.61	2.51	0.71
1383	1110					3.56	3.34	3.01	1.75
T Final	K	1402	1402	1397	1397	1386	1386	1380	1380
Datapoint	C	1129	1129	1124	1124	1113	1113	1107	1107

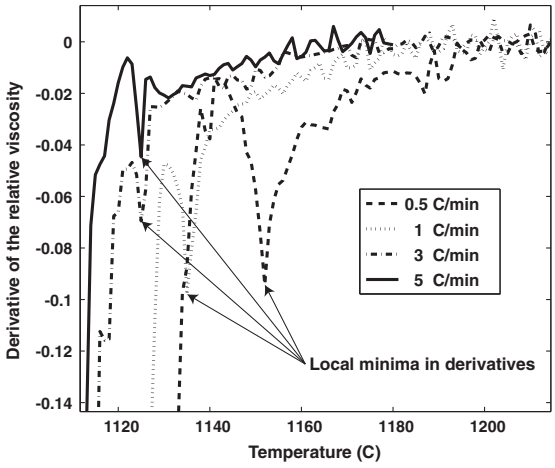

Fig. 7. derivative of the relative viscosity data with respect to temperature, zoomed to the change-zone related to crystallization. The derivatives of the relative viscosity data show local changes in crystallization intensity during cooling. Decreasing values indicate more rapid crystallization and therewith increase in relative viscosity, whereas increasing values indicate a decrease in crystallization intensity. All datasets show one or more local minima (onset of decreasing crystallization intensity). The location of these minima shift to lower temperatures with increasing cooling rate.

therewith lowering its viscosity. Our data show that the effect of increasing crystal fraction dominates any rheological effect of the release of latent heat during crystallization.

5. DISCUSSION

5.1. Cooling rate dependence of disequilibrium kinetics and the effect of latent heat on the system's rheology

We have shown that faster cooling rates drive the onset of crystallization to lower temperatures and that the intensity of crystallization events (measured through both the release of thermal energy and the increase in apparent viscosity) increases with increasing undercooling of the basaltic melt studied here. These observations are consistent with long-standing concepts of crystallization kinetics of supercooled basaltic liquids, where with increasing undercooling both crystal nucleation rates and growth intensities increase at near liquidus conditions (Gibb, 1974; Walker et al., 1976; Coish and Taylor, 1979; Lofgren, 1980; Cashman, 1993; Lange et al., 1994; Hammer, 2006; Mollo et al., 2011; Arzilli and Carroll, 2013; Vetere et al., 2013). This behavior is a result of the time dependence of the nucleation and growth processes whereby faster cooling yields greater deviations of the system from its thermodynamic equilibrium to higher degrees of undercooling. Crystal growth rates are also dependent on the absolute viscosity of the system through the diffusivity of individual ions within the melt, see Vetere et al. (2015) and references therein for a broad dataset and recent review.

The influence of the release of latent heat on the flow properties of magmas has been subject to theoretical studies concerning the emplacement of magmas and lava flows (Settle, 1979; Lipman et al., 1985; Dragoni and Tallarico, 1994). These authors describe and model a decrease in bulk viscosity through the heating of the melt during crystallization. We present the first experimental dataset tracking the variations of both properties in a melt subjected to cooling conditions similar to those observed in nature. Our data show that although the release of latent heat may cause delay in the cooling of a melt or even lead to recalescence, i.e. re-heating of the melt as described by Whittington and Sehlke (2015) and Blundy et al. (2006), the effect of an increased solid fraction dominates the influence of the release of latent heat on the flow properties of the suspension. This results in a steadily increasing apparent viscosity of the system. The measured relative increase in sample temperature of 4 K would result in a lower melt viscosity of 0.03 and 0.04 log units at 1100 and 1200 °C, respectively (estimated using the GRD model). This finding holds in a similar way also for any potential effect of viscous heating in lavas under disequilibrium conditions. At constant temperature, viscous heating could nonetheless introduce a decrease in bulk viscosity.

5.2. Importance of disequilibrium rheological data for accurate interpretation of lava flow emplacement and magma migration

Modeling of sub-liquidus rheology for volcanological applications has almost exclusively been based on the assumption of thermodynamic equilibrium between melt and crystals (Ishihara et al., 1990; Harris and Rowland, 2001; Saar et al., 2001; Costa and Macedonio, 2005a; Del Negro et al., 2008; Herault et al., 2009; Vona et al., 2011; Fujita and Nagai, 2015). It is commonly assumed that any changes in rheological properties occur instantaneously with changes in temperature and, therewith, crystal content of the magma/lava.

All existing experimental studies, however, show a significant delay in changing physical properties that strongly depends on how far and how fast a melt is cooled below its liquidus temperature (Mollo et al., 2011; Arzilli and Carroll, 2013). This is a result of changes in the crystallization kinetics under disequilibrium conditions. In isothermal regimes, this translates into varying "incubation times" of the liquids' viscosity before the onset of crystallization and changing suspension viscosity (Vona et al., 2011, 2013; Chevrel et al., 2015; Campagnola et al., 2016; Soldati et al., 2016). In non-isothermal regimes, this results in a cooling rate dependent shift of the rheological cut off temperature as shown in this study and also in Giordano et al. (2007).

Although interesting for magmatic systems at constant (or close to constant) temperature, such as convecting magma chambers or the interior of lava lakes, isothermal sub-liquidus experiments are not directly applicable to the dynamic thermal conditions present in lava flows or during magma transport within narrow dykes, where heat loss is significant.

For a given temperature, isothermal experiments return systematically higher viscosities than constant cooling rheology experiments. This is because they reach equilibrium

crystal contents which are, in all cases, higher than the crystal content present in constant cooling experiments at the same temperature. The same applies for rheological models based on equilibrium thermodynamics like using MELTS in combination with two phase rheological models such as Mader et al. (2013). However, in constant cooling experiments, like the ones presented here, it becomes obvious that the actual viscosity of a lava/magma under constant cooling conditions is lower than the estimate of the equilibrium viscosity at the same temperature. This is likely the reason why lava flow runout distances are often underestimated.

Further, experimental studies of the crystallization kinetics of natural melts under constant cooling conditions but in the absence of deformation, like those presented in Lange et al. (1994), are unable to reproduce natural processes, where deformation of the melt leads to significant changes in crystallization kinetics (Kouchi et al., 1986; Vona and Romano, 2013).

It has also been subject to debate whether and how much the release of latent heat of crystallization and or viscous heating influences the rheology of crystallizing melts. Some modeling and experimental data suggest that it may contribute to keep magmas/lavas flowing for longer (Settle, 1979; Costa and Macedonio, 2005b; Cordonnier et al., 2012). However, the new and unique data presented here, combining thermal and rheological measurements, show that the effect of increasing crystal content dominates any other effect under constant cooling conditions for viscosity regimes relevant to lava flow emplacement (i.e. $<10^5$ Pa s).

Flow emplacement models often incorporate a yield strength parameter that allows for the lava to stop flowing in the model although it is not fully solidified. The presented experimental dataset is the first to quantify the systematic, crystallization-induced rheological and thermal evolution of a basaltic melt undergoing a range of cooling rates relevant to natural conditions and to track this evolution until the systems' rheological "cut-off" is reached, where the apparent viscosity of the suspension rises drastically, (i.e. it rheologically solidifies).

Our data show that this cut-off is dependent on the cooling rate of the lava. In order to systematically describe the influence of cooling rate on the rheologic cut-off we plot the temperatures at which each experimental dataset passes a viscosity threshold of 10^3 Pa s (Fig. 8). Beyond this point, all datasets reach the measurement limit within few degrees of cooling, i.e. the sample solidifies. The data show a logarithmic decay of the cut-off temperature as a function of cooling rate. We fit a model to the data that describes the cut-off temperature as a function of cooling rate with an *R*-squared value of 0.9987. Extrapolation of the data using this model suggests that further increasing cooling rate would have little effect on this rheologic threshold, whereas decreasing cooling rates would further increase the temperature at which this threshold is reached. This is due to the longer time spent at higher temperatures, allowing for crystal growth under near equilibrium conditions. However, since the model describes a crystallization induced rheologic threshold, it is important to note that the model is only valid at sub-liquidus temperatures and non-equilibrium conditions.

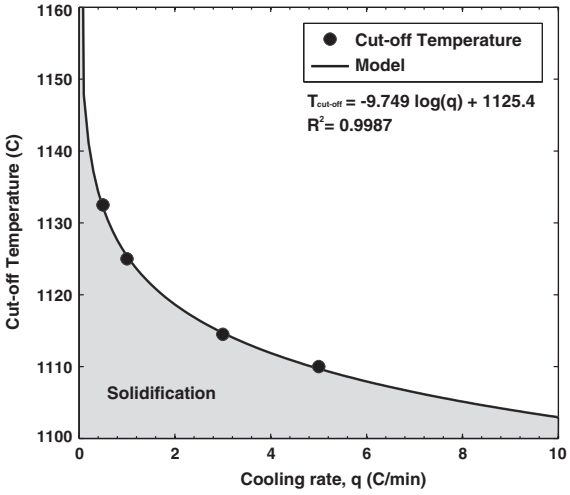

Fig. 8. Cooling rate dependence of the solidification threshold. Plot of the rheological threshold temperature versus cooling rate. The temperature at which the rheological threshold of 10^3 Pa s is reached decreases with increasing cooling rate. Beyond this threshold the effective viscosity of the lava reaches the measurement limit within few degrees of cooling, i.e. the lava solidifies. The gray shaded area delineates the solidification field.

Incorporating such data in lava flow models would allow for the concept of yield strength to be replaced by a melt specific rheological cut off. This would lead to a more realistic description of the magmas/lavas rheological evolution and therewith better ability to forecast their emplacement.

5.3. Limitations of the method

The experiments performed in this study are carried out on degassed melts at ambient pressures, in air and the melts are bubble free. All these parameters are important to consider when interpreting the experimental data with respect to natural systems. They influence the pure melt viscosity and its crystallization kinetics to varying degrees. The water content of the melt has the largest effect, where a few weight percent of water can decrease the melt viscosity by up to 6 orders of magnitude for rhyolitic systems and up to 1.5 orders of magnitude for basaltic systems (Friedman et al., 1963; Dingwell and Mysen, 1985; Holtz et al., 1992; Richet et al., 1996; Whittington et al., 2000; Giordano and Dingwell, 2003; Robert et al., 2008; Giordano et al., 2008a, 2008b, 2009). Vesicles can both increase and decrease the bulk viscosity of a suspension, depending on their capillary number (Llewellin et al., 2002; Llewellin and Manga, 2005; Mader et al., 2013). The redox state of the melt may also influence the melt viscosity and its crystallization evolution through changes in the melt structure resulting from iron acting as network-former or -modifier. However, the absolute difference in melt viscosity resulting from changes in redox state is low with respect to that related to the presence of dissolved water or bubbles (Dingwell, 1991; Bouhifd et al., 2004; Chevrel et al., 2013, 2014).

6. CONCLUSIONS

Based on the data presented above and the accompanying analytical results we draw the following conclusions:

1. The effect of increasing crystal fraction dominates any effect of latent heat or viscous heating under constant cooling conditions, resulting in the rheological death of a lava flow.
2. The new device and method presented here allow, for the first time, *direct* measurement of sample temperature and -gradients within the sample during high temperature concentric cylinder viscometry.
3. This allows for more precise measurements of the temperature dependent viscosity of silicate melts, especially in dynamic temperature space.
4. The presented device and method open an entirely new field of studies through the combined measurement of the rheological and thermal evolution of crystallizing melts. Such measurements are of key importance to advance our understanding of disequilibrium processes operating during lava flow emplacement as well as magma ascent and migration in the earth's crust.
5. The dataset presented here is a first step in building a broad experimental database of the evolution of the transport properties of silicate melts under disequilibrium conditions.
6. The presented data can be employed to more accurately constrain the results of physical property based models of lava flow emplacement.

ACKNOWLEDGEMENTS

We would like to thank Werner Ertel-Ingrisch and Kai-Uwe Hess for support in the laboratory and interesting discussions during the experimental campaign. Stephan Kolzenburg and Daniele Giordano acknowledge financial support for this research from grants awarded through the Fondazione CRT, grant title "*Implementazione di un laboratorio per lo studio delle proprietà reologiche di geomateriali e fusi silicatici a bassa, media ed alta temperatura*", and further funding by the *Compagnia San Paolo*, an ERASMUS Traineeship and the local research project (Giordano, 2012) of the University of Torino, titled: "Integrated field, laboratory and remote sensing applications investigation to determine rheological models of the emplacement of low-viscosity lava flows in active volcanic areas" for providing funding for this research. Westmount Public Library is also thanked for providing a very welcoming writing environment. The presented research was partially funded by an ERC Advanced Investigator Grant (EVOKES – No. 247076) held by Prof. Dingwell.

REFERENCES

Arzilli F. and Carroll M. R. (2013) Crystallization kinetics of alkali feldspars in cooling and decompression-induced crystallization experiments in trachytic melt. *Contrib. Miner. Petrol.* **166**(4), 1011–1027.

Blundy J., Cashman K. and Humphreys M. (2006) Magma heating by decompression-driven crystallization beneath andesite volcanoes. *Nature* **443**(7107), 76–80.

Bouhifd M. A., Richet P., Besson P., Roskosz M. and Ingrin J. (2004) Redox state, microstructure and viscosity of a partially crystallized basalt melt. *Earth Planet. Sci. Lett.* **218**(1), 31–44.

Calvari S. and Pinkerton H. (1998) Formation of lava tubes and extensive flow field during the 1991–1993 eruption of Mount Etna. *J. Geophys. Res.: Solid Earth (1978–2012)* **103**(B11), 27291–27301.

Campagnola S., Vona A., Romano C. and Giordano G. (2016) Crystallization kinetics and rheology of leucite-bearing tephriphonolite magmas from the Colli Albani volcano (Italy). *Chem. Geol.* **424**, 12–29.

Cashman K. (1993) Relationship between plagioclase crystallization and cooling rate in basaltic melts. *Contrib. Miner. Petrol.* **113**(1), 126–142.

Cashman K. V., Thornber C. and Kauahikaua J. P. (1999) Cooling and crystallization of lava in open channels, and the transition of Pāhoehoe Lava to'A'ā. *Bull. Volcanol.* **61**(5), 306–323.

Cashman K., Soule S., Mackey B., Deligne N., Deardorff N. and Dietterich H. (2013) How lava flows: new insights from applications of lidar technologies to lava flow studies. *Geosphere* **9**(6), 1664–1680.

Castruccio A. and Contreras M. A. (2016) The influence of effusion rate and rheology on lava flow dynamics and morphology: a case study from the 1971 and 1988–1990 eruptions at Villarrica and Lonquimay volcanoes, Southern Andes of Chile. *J. Volcanol. Geoth. Res.*

Chevrel M. O., Giordano D., Potuzak M., Courtial P. and Dingwell D. B. (2013) Physical properties of $CaAl_2Si_2O_8$–$CaMgSi_2O_6$–FeO–Fe_2O_3 melts: analogues for extra-terrestrial basalt. *Chem. Geol.* **346**, 93–105.

Chevrel M. O., Baratoux D., Hess K.-U. and Dingwell D. B. (2014) Viscous flow behavior of tholeiitic and alkaline Fe-rich martian basalts. *Geochim. Cosmochim. Acta* **124**, 348–365.

Chevrel M. O., Cimarelli C., deBiasi L., Hanson J. B., Lavallée Y., Arzilli F. and Dingwell D. B. (2015) Viscosity measurements of crystallizing andesite from Tungurahua volcano (Ecuador). *Geochem. Geophys. Geosyst.*

Coish R. and Taylor L. A. (1979) The effects of cooling rate on texture and pyroxene chemistry in DSDP Leg 34 basalt: a microprobe study. *Earth Planet. Sci. Lett.* **42**(3), 389–398.

Cordonnier B., Schmalholz S., Hess K. U. and Dingwell D. (2012) Viscous heating in silicate melts: an experimental and numerical comparison. *J. Geophys. Res.: Solid Earth (1978–2012)* **117** (B2).

Costa A. and Macedonio G. (2005a) Computational modeling of lava flows: a review. *Geol. Soc. Am. Spec. Pap.* **396**, 209–218.

Costa A. and Macedonio G. (2005b) Viscous heating effects in fluids with temperature-dependent viscosity: triggering of secondary flows. *J. Fluid Mech.* **540**, 21–38.

Del Negro C., Fortuna L., Herault A. and Vicari A. (2008) Simulations of the 2004 lava flow at Etna volcano using the magflow cellular automata model. *Bull. Volcanol.* **70**(7), 805–812.

Dingwell D. B. (1986) Viscosity-temperature relationships in the system $Na_2Si_2O_5$-$Na_4Al_2O_5$. *Geochim. Cosmochim. Acta* **50**(6), 1261–1265.

Dingwell D. B. (1989) Shear viscosities of ferrosilicate liquids. *Am. Mineral.*, 1038–1044 (9–10).

Dingwell D. (1991) Redox viscometry of some Fe-bearing silicate melts. *Am. Mineral.* **76**(9–10), 1560–1562.

Dingwell D. B. and Mysen B. O. (1985) Effects of water and fluorine on the viscosity of albite melt at high pressure: a preliminary investigation. *Earth Planet. Sci. Lett.* **74**(2), 266–274.

Dingwell D. B. and Virgo D. (1987) The effect of oxidation state on the viscosity of melts in the system Na_2O-FeO-Fe_2O_3-SiO_2. *Geochim. Cosmochim. Acta* **51**(2), 195–205.

Dingwell D. B. and Virgo D. (1988) Viscosities of melts in the Na_2O–FeO–Fe_2O_3–SiO_2 system and factors controlling relative viscosities of fully polymerized silicate melts. *Geochim. Cosmochim. Acta*, 395–403 (2).

Dragoni M. and Tallarico A. (1994) The effect of crystallization on the rheology and dynamics of lava flows. *J. Volcanol. Geoth. Res.* **59**(3), 241–252.

Flynn L. P. and Mouginis-Mark P. J. (1992) Cooling rate of an active Hawaiian lava flow from nighttime spectroradiometer measurements. *Geophys. Res. Lett.* **19**(17), 1783–1786.

Flynn L. and Mouginis-Mark P. (1994) Temperature of an active lava channel from spectral measurements, Kilauea Volcano, Hawaii. *Bull. Volcanol.* **56**(4), 297–301.

Friedman I., Long W. and Smith R. L. (1963) Viscosity and water content of rhyolite glass. *J. Geophys. Res.* **68**, 6523–6535.

Fujita E. and Nagai M. (2015) LavaSIM: its physical basis and applicability. *Geol. Soc., London, Spec. Publ.* **426**(SP426), 14.

Gamble R. P. and Taylor L. A. (1980) Crystal/liquid partitioning in augite: effects of cooling rate. *Earth Planet. Sci. Lett.* **47**(1), 21–33.

Gibb F. G. (1974) Supercooling and the crystallization of plagioclase from a basaltic magma. *Mineral. Mag.* **39**(306), 641–653.

Giordano D. and Dingwell D. (2003) Viscosity of hydrous Etna basalt: implications for Plinian-style basaltic eruptions. *Bull. Volcanol.* **65**(1), 8–14.

Giordano D., Polacci M., Longo A., Papale P., Dingwell D., Boschi E. and Kasereka M. (2007) Thermo-rheological magma control on the impact of highly fluid lava flows at Mt. Nyiragongo. *Geophys. Res. Lett.* **34**(6).

Giordano D., Potuzak M., Romano C., Dingwell D. B. and Nowak M. (2008a) Viscosity and glass transition temperature of hydrous melts in the system $CaAl_2Si_2O_8$–$CaMgSi_2O_6$. *Chem. Geol.* **256**(3–4), 203–215.

Giordano D., Russell J. K. and Dingwell D. B. (2008b) Viscosity of magmatic liquids: a model. *Earth Planet. Sci. Lett.* **271**(1–4), 123–134.

Giordano D., Ardia P., Romano C., Dingwell D. B., Di Muro A., Schmidt M. W., Mangiacapra A. and Hess K.-U. (2009) The rheological evolution of alkaline Vesuvius magmas and comparison with alkaline series from the Phlegrean Fields, Etna, Stromboli and Teide. *Geochim. Cosmochim. Acta* **73**(21), 6613–6630.

Giordano D., Polacci M., Papale P. and Caricchi L. (2010) Rheological control on the dynamics of explosive activity in the 2000 summit eruption of Mt. Etna. *Solid Earth*.

Gottsmann J., Giordano D. and Dingwell D. B. (2002) Predicting shear viscosity during volcanic processes at the glass transition: a calorimetric calibration. *Earth Planet. Sci. Lett.* **198**(3), 417–427.

Gualda G. A. and Ghiorso M. S. (2015) MELTS_Excel: a Microsoft Excel-based MELTS interface for research and teaching of magma properties and evolution. *Geochem. Geophys. Geosyst.* **16**(1), 315–324.

Hammer J. E. (2006) Influence of fO_2 and cooling rate on the kinetics and energetics of Fe-rich basalt crystallization. *Earth Planet. Sci. Lett.* **248**(3), 618–637.

Harris A. J. and Rowland S. (2001) FLOWGO: a kinematic thermo-rheological model for lava flowing in a channel. *Bull. Volcanol.* **63**(1), 20–44.

Harris A., Bailey J., Calvari S. and Dehn J. (2005) Heat loss measured at a lava channel and its implications for down-channel cooling and rheology. *Geol. Soc. Am. Spec. Pap.* **396**, 125–146.

Harris A. J., Dehn J. and Calvari S. (2007) Lava effusion rate definition and measurement: a review. *Bull. Volcanol.* **70**(1), 1–22.

Herault A., Vicari A., Ciraudo A. and Del Negro C. (2009) Forecasting lava flow hazards during the 2006 Etna eruption: using the MAGFLOW cellular automata model. *Comput. Geosci.* **35**(5), 1050–1060.

Hess K.-U., Cordonnier B., Lavallée Y. and Dingwell D. B. (2008) Viscous heating in rhyolite: an in situ experimental determination. *Earth Planet. Sci. Lett.* **275**(1–2), 121–126.

Hess K.-U. and Dingwell D. B. (1996) Viscosities of hydrous leucogranitic melts: a non-Arrhenian model. *Am. Mineral.* **81**, 1297–1300.

Hess K., Dingwell D. and Webb S. (1995) The influence of excess alkalis on the viscosity of a haplogranitic melt. *Am. Mineral.* **80**(3), 297–304.

Holtz F., Behrens H., Dingwell D. B. and Taylor R. P. (1992) Water solubility in aluminosilicate melts of haplogranite composition at 2 kbar. *Chem. Geol.* **96**(3–4), 289–302.

Hon K., Kauahikaua J., Denlinger R. and Mackay K. (1994) Emplacement and inflation of pahoehoe sheet flows: observations and measurements of active lava flows on Kilauea Volcano, Hawaii. *Geol. Soc. Am. Bull.* **106**(3), 351–370.

Hon K., Gansecki C. and Kauahikaua J. (2003) The Transition from'A'a to Pahoehoe Crust on Flows Emplaced During the Pu'u'6'6-Kupaianaha Eruption. *U.S. Geol. Surv. Prof. Pap.* **1676**, 89.

Hoover S. R., Cashman K. V. and Manga M. (2001) The yield strength of subliquidus basalts — experimental results. *J. Volcanol. Geoth. Res.* **107**(1–3), 1–18.

Hui H. and Zhang Y. (2007) Toward a general viscosity equation for natural anhydrous and hydrous silicate melts. *Geochim. Cosmochim. Acta* **71**(2), 403–416.

Huppert H. E., Sparks R. S. J., Turner J. S. and Arndt N. T. (1984) Emplacement and cooling of komatiite lavas. *Nature* **309**(5963), 19–22.

Ishibashi H. (2009) Non-Newtonian behavior of plagioclase-bearing basaltic magma: subliquidus viscosity measurement of the 1707 basalt of Fuji volcano, Japan. *J. Volcanol. Geoth. Res.* **181**(1–2), 78–88.

Ishibashi H. and Sato H. (2007) Viscosity measurements of subliquidus magmas: alkali olivine basalt from the Higashi-Matsuura district, Southwest Japan. *J. Volcanol. Geoth. Res.* **160**(3–4), 223–238.

Ishihara K., Iguchi M. and Kamo K. (1990) *Numerical simulation of lava flows on some volcanoes in Japan. Lava flows and domes*. Springer, pp. 174–207.

Kauahikaua J., Cashman K. V., Mattox T. N., Heliker C. C., Hon K. A., Mangan M. T. and Thornber C. R. (1998) Observations on basaltic lava streams in tubes from Kilauea Volcano, island of Hawai'i. *J. Geophys. Res.: Solid Earth (1978–2012)* **103**(B11), 27303–27323.

Kouchi A., Tsuchiyama A. and Sunagawa I. (1986) Effect of stirring on crystallization kinetics of basalt: texture and element partitioning. *Contrib. Miner. Petrol.* **93**(4), 429–438.

Kress V. C. and Carmichael I. S. (1991) The compressibility of silicate liquids containing Fe2O3 and the effect of composition, temperature, oxygen fugacity and pressure on their redox states. *Contrib. Miner. Petrol.* **108**(1–2), 82–92.

Lange R. A., Cashman K. V. and Navrotsky A. (1994) Direct measurements of latent heat during crystallization and melting of a ugandite and an olivine basalt. *Contrib. Miner. Petrol.* **118**(2), 169–181.

Lipman P. and Banks N. (1987) AA flow dynamics, Mauna Loa 1984. *US Geol. Surv. Prof. Pap* **1350**, 1527–1567.

Lipman P. W., Banks N. G. and Rhodes J. M. (1985) Degassing-induced crystallization of basaltic magma and effects on lava rheology. *Nature* **317**(6038), 604–607.

Llewellin E., Mader H. and Wilson S. (2002) The rheology of a bubbly liquid. In *Proceedings of the Royal Society of London A: Mathematical, Physical and Engineering Sciences, 458*. The Royal Society, pp. 987–1016.

Llewellin E. and Manga M. (2005) Bubble suspension rheology and implications for conduit flow. *J. Volcanol. Geoth. Res.* **143**(1), 205–217.

Lofgren, G. (1980) Experimental studies on the dynamic crystallization of silicate melts. Physics of magmatic processes, 487.

Long P. E. and Wood B. J. (1986) Structures, textures, and cooling histories of Columbia River basalt flows. *Geol. Soc. Am. Bull.* **97**(9), 1144–1155.

Mader H. M., Llewellin E. W. and Mueller S. P. (2013) The rheology of two-phase magmas: a review and analysis. *J. Volcanol. Geotherm. Res.* **257**, 135–158.

Mauro J. C., Yue Y., Ellison A. J., Gupta P. K. and Allan D. C. (2009) Viscosity of glass-forming liquids. *Proc. Natl. Acad. Sci. U.S.A.* **106**(47), 19781–19784.

Meerlender G. (1975) Erstes Standardglas der Deutschen Glastechnischen Gesellschaft und Realisierung der Viskositätsskala bei hohen Temperaturen. *Rheol. Acta* **14**(3), 279–290.

Mollo S., Putirka K., Iezzi G., Del Gaudio P. and Scarlato P. (2011) Plagioclase–melt (dis) equilibrium due to cooling dynamics: implications for thermometry, barometry and hygrometry. *Lithos* **125**(1), 221–235.

Mysen B. R. O. and Virgo D. (1978) Influence of pressure, temperature, and bulk composition on melt structures in the system $NaAlSi_2O_6$–$NaFe^{3+}Si_2O_6$. *Am. J. Sci.* **278**(9), 1307–1322.

Peterson D. W. and Swanson D. A. (1974) Observed formation of lava tubes during 1970–71 at Kilauea Volcano, Hawaii. *Stud. Speleol.* **2**(6), 209–222.

Pinkerton H. and Norton G. (1995) Rheological properties of basaltic lavas at sub-liquidus temperatures: laboratory and field measurements on lavas from Mount Etna. *J. Volcanol. Geoth. Res.* **68**(4), 307–323.

Pinkerton H. and Sparks R. S. J. (1978) Field measurements of the rheology of lava. *Nature* **276**(5686), 383–385.

Richet P., Lejeune A.-M., Holtz F. and Roux J. (1996) Water and the viscosity of andesite melts. *Chem. Geol.* **128**(1), 185–197.

Robert B., Harris A., Gurioli L., Médard E., Sehlke A. and Whittington A. (2014) Textural and rheological evolution of basalt flowing down a lava channel. *Bull. Volcanol.* **76**(6), 1–21.

Robert G., Russell J. K., Giordano D. and Romano C. (2008) High-temperature deformation of volcanic materials in the presence of water. *Am. Min.* **93**(1), 74–80.

Russell J., Giordano D. and Dingwell D. (2003) High-temperature limits on viscosity of non-Arrhenian silicate melts. *Am. Mineral.* **88**(8–9), 1390–1394.

Russell J. K., Giordano D., Dingwell D. B. and Kai-Uwe H. (2002) Modelling the non-Arrhenian rheology of silicate melts Numerical considerations. *Eur. J. Mineral.* **14**(2), 417–427.

Ryerson F. J., Weed H. C. and Piwinskii A. J. (1988a) Rheology of subliquidus magmas: 1. Picritic compositions. *J. Geophys. Res.: Solid Earth* **93**(B4), 3421–3436.

Saar M. O., Manga M., Cashman K. V. and Fremouw S. (2001) Numerical models of the onset of yield strength in crystal–melt suspensions. *Earth Planet. Sci. Lett.* **187**(3), 367–379.

Sarbas B. and Nohl U. (2008) The GEOROC database as part of a growing geoinformatics network. *Geoinformatics*.

Sato H. (2005) Viscosity measurement of subliquidus magmas: 1707 basalt of Fuji volcano. *J. Mineral. Petrol. Sci.* **100**(4), 133–142.

Sehlke A. and Whittington A. G. (2015) Rheology of lava flows on Mercury: an analog experimental study. *J. Geophys. Res.: Planets* **120**(11), 1924–1955.

Sehlke A., Whittington A., Robert B., Harris A., Gurioli L. and Médard E. (2014) Pahoehoe to ‘a‘a transition of Hawaiian lavas: an experimental study. *Bull. Volcanol.* **76**(11), 1–20.

Settle M. (1979) Lava rheology: thermal buffering produced by the latent heat of crystallization. *Lunar and Planetary Science Conference* **10**, 1107–1109.

Shaw H., Wright T., Peck D. and Okamura R. (1968) The viscosity of basaltic magma; an analysis of field measurements in Makaopuhi lava lake, Hawaii. *Am. J. Sci.* **266**(4), 225–264.

Soldati A., Sehlke A., Chigna G. and Whittington A. (2016) Field and experimental constraints on the rheology of arc basaltic lavas: the January 2014 Eruption of Pacaya (Guatemala). *Bull. Volcanol.* **78**(6), 1–19.

Sparks R., Pinkerton H. and Hulme G. (1976) Classification and formation of lava levees on Mount Etna, Sicily. *Geology* **4**(5), 269–271.

Stein D. J. and Spera F. J. (1992) Rheology and microstructure of magmatic emulsions: theory and experiments. *J. Volcanol. Geoth. Res.* **49**(1), 157–174.

Stevenson R., Dingwell D. B., Webb S. and Bagdassarov N. (1995) The equivalence of enthalpy and shear stress relaxation in rhyolitic obsidians and quantification of the liquid-glass transition in volcanic processes. *J. Volcanol. Geoth. Res.* **68**(4), 297–306.

Tammann G. and Hesse W. (1926) Die Abhängigkeit der Viscosität von der Temperatur bie unterkühlten Flüssigkeiten. *Zeitschrift für anorganische und allgemeine Chemie* **156**(1), 245–257.

Vetere F., Iezzi G., Behrens H., Cavallo A., Misiti V., Dietrich M., Knipping J., Ventura G. and Mollo S. (2013) Intrinsic solidification behaviour of basaltic to rhyolitic melts: a cooling rate experimental study. *Chem. Geol.* **354**, 233–242.

Vetere F., Iezzi G., Behrens H., Holtz F., Ventura G., Misiti V., Cavallo A., Mollo S. and Dietrich M. (2015) Glass forming ability and crystallisation behaviour of sub-alkaline silicate melts. *Earth Sci. Rev.* **150**, 25–44.

Vona A. and Romano C. (2013) The effects of undercooling and deformation rates on the crystallization kinetics of Stromboli and Etna basalts. *Contrib. Miner. Petrol.* **166**(2), 491–509.

Vona A., Romano C., Dingwell D. B. and Giordano D. (2011) The rheology of crystal-bearing basaltic magmas from Stromboli and Etna. *Geochim. Cosmochim. Acta* **75**(11), 3214–3236.

Vona A., Romano C., Giordano D. and Russell J. K. (2013) The multiphase rheology of magmas from Monte Nuovo (Campi Flegrei, Italy). *Chem. Geol.* **346**, 213–227.

Walker D., Kirkpatrick R., Longhi J. and Hays J. (1976) Crystallization history of lunar picritic basalt sample 12002: phase-equilibria and cooling-rate studies. *Geol. Soc. Am. Bull.* **87**(5), 646–656.

Webb S. L. and Dingwell D. B. (1990) Non-Newtonian rheology of igneous melts at high stresses and strain rates: experimental results for rhyolite, andesite, basalt, and nephelinite. *J. Geophys. Res.* **95**(B10), 15695–15701.

Whittington A., Richet P. and Holtz F. (2000) Water and the viscosity of depolymerized aluminosilicate melts. *Geochim. Cosmochim. Acta* **64**(21), 3725–3736.

Whittington A. and Sehlke A. (2015) *Recalescence in Silicate Melts: More Than Just a Flash in the Pan? AGU Fall Meeting 2015*. AGU, San Francisco, USA.

Witter J. B. and Harris A. J. (2007) Field measurements of heat loss from skylights and lava tube systems. *J. Geophys. Res.: Solid Earth (1978–2012)* **112**(B1).

Wright T. L. and Okamura R. T. (1977) *Cooling and crystallization of tholeiitic basalt, 1965 Makaopuhi lava lake*. US Government Printing Office, Hawaii.

Associate editor: Michael J. Toplis